

Transport and Fate of Reactive Trace Gases in Red Spruce Needles. 2. Interpretations of Flux Experiments Using Gas Transport Theory

Candis S. Clalborn,^{*†} Ruben G. Carbonell,[‡] and Viney P. Aneja[§]

Laboratory for Atmospheric Research, Department of Civil and Environmental Engineering, Washington State University, Pullman, Washington 99164-2910, Department of Chemical Engineering, North Carolina State University, Raleigh, North Carolina 27695-7905, and Department of Marine, Earth, and Atmospheric Sciences, North Carolina State University, Raleigh, North Carolina 27695-8208

A mathematical description of the multicomponent transport of gaseous species into needles of conifer trees is presented. Detailed physiology of the stomatal zone is taken into account, and diffusion through the atmospheric boundary layer, wax-filled antechamber, stomata, and substomatal cavity are described starting from the fundamental equations for multicomponent gas diffusion. The model was used to analyze the results from two sets of exposure experiments in which red spruce saplings were exposed to gas-phase H₂O₂ or to a combination of H₂O₂, SO₂, and O₃. Model calculations indicate that the wax-filled antechamber may provide a porous zone in which water can condense, thus protecting the sensitive inner tissues below the stomata from exposure to water-soluble, toxic, trace gases (such as SO₂ and H₂O₂). The model was found to be sensitive to the accuracy of measurements of leaf temperature, dewpoint temperature of the chamber inlet and exit air, and gas flow rate and may provide some insight into the role of atmospheric pollutants in forest decline.

I. Introduction

Understanding the gas exchange between the atmosphere and plants is important to both atmospheric and plant scientists. Annual crop loss due to O₃ damage, for example, has been estimated to be on the order of 2-5 billion dollars in the United States alone (1). Circumstantial evidence also links O₃ exposure to high elevation spruce/fir forest decline in the United States and in Central Europe (2). Vegetation also plays an important role in the chemistry of the atmosphere. Many plant species have been found to be a source of highly reactive alkenes (e.g., ref 3), trace gases which are important O₃ precursors. Vegetation also acts as a sink for many air pollutants (e.g., ref 4). For some species such as H₂O₂, losses to vegetative surfaces may be one of the most important loss processes (5). Therefore, the development of a fundamental model which describes the exchange of gases between plants and the environment would benefit both the plant science and atmospheric science communities.

Traditionally, the exposure of a plant to an atmospheric trace gas is characterized by the deposition velocity model (4), which inherently assumes that the leaf's internal concentration of the pollutant, C_{int} , is zero (6, 7), so that

$$Q = V_d(C_{amb} - C_{int}) \approx V_d C_{amb} \quad (1)$$

where Q is the gas flux to the leaf, V_d is the deposition

velocity, and C_{amb} is the ambient concentration. The deposition velocity (or resistance) model does not address the effects of the trace gas solubility or chemical reactions occurring in plant tissue. It also ignores the net convective flux of gases out of the leaf which develops when the plant is transpiring (8). The modified resistance model of Von Caemmerer and Farquhar (9), which takes into account the net flow of water vapor out of the leaf for calculating the intercellular CO₂ concentration, applies only to the system of H₂O, CO₂, and air.

The Stefan-Maxwell equation, upon which the modified resistance model is based (9), assumes that the primary diffusion mechanism is molecular. In small volumes, however, molecule-wall collisions (Knudsen diffusion) may also contribute to diffusion. The Stefan-Maxwell equation can be modified to include the effects of the wall, so that the resulting equation includes Knudsen as well as molecular diffusion (10, 11)

$$-\frac{1}{RT} \frac{\partial P_i}{\partial z} = \frac{N_i^D}{D_{ii}^K} + \sum_{j=1, j \neq i}^n \frac{x_j N_j^D - x_i N_j^D}{D_{ij}} \quad (2)$$

where N_i^D is the diffusive molar flux of species i ; D_{ij} is the molecular diffusion coefficient of species i with respect to j ; D_{ii}^K is the Knudsen diffusivity of i ; x_i and P_i are the mole fraction and partial pressure of species i , respectively; T is the absolute temperature; and R is the universal gas constant. This form of the Stefan-Maxwell equation was applied to the problem of diffusion in the stomatal region, where the stomatal pore diameter may approach the molecular mean free path so that Knudsen diffusion can become important (12). In ref 12, gas diffusion through the stomatal pore was treated as one-dimensional, multicomponent diffusion through a small capillary. By making some simplifying assumptions, ignoring chemical reactions in the leaf, and expressing gradients in finite-difference form, the resulting model presented in ref 12 is valid for no more than three gases.

In estimating the mass-transfer resistance due to the laminar boundary layer next to the leaf, unusual leaf geometries (aside from flat plate geometry) have been neglected in most of the modeling efforts reported to date. Other stomatal configurations (e.g., stomata not located at the leaf surface) are also typically neglected. For many conifers, however, the leaf is not flat but is approximately needle-shaped and is covered with a waxy surface into which the stomata are sunken.

In this work, we use gas transport theory to examine the transport of gases into conifer needles, taking into account the geometry of the spruce needle and the physiology of its stomatal zone. The assumption of a flat plate geometry is relaxed for the calculation of the boundary layer resistance. Reactive trace gases are considered by taking

* Author to whom correspondence should be addressed.

† Washington State University.

‡ Department of Chemical Engineering, North Carolina State University.

§ Department of Marine, Earth, and Atmospheric Sciences, North Carolina State University.

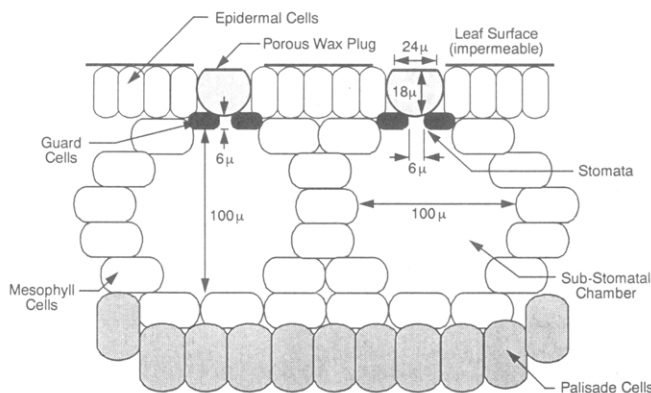


Figure 1. Stomatal zone of conifer needle. The figure shows cross-sectional area of stomata, for one side of needle, only (spruce needle is four-sided). The guard cells are below the epidermal cells, and the stomata are "sunken" in the cuticular wax. The "antechamber" above the stomata is filled with a porous medium comprised of finely divided wax rodlets. Below the stomata is the substomatal chamber, which is filled with air. Mesophyll cells form the boundary around the substomatal chamber. The mesophyll cell wall is comprised largely of water. Inside the cell wall is the cell membrane, which is vulnerable to oxidant attack (e.g., ozone damage occurs at the cell membrane). Dimensions taken from ref 19.

into account chemical reactions at the cell wall. The modified Stefan–Maxwell equations are solved directly so that the model can accommodate as many gases as desired. By solving the equations exactly, we are also able to incorporate detailed stomatal geometry, therefore making the model applicable to a wide variety of plant species. We use for illustration the red spruce, whose stomatal geometry differs considerably from that of the typical flat-leaved plant. Our approach is to treat the stomatal zone as four coupled regions with continuity of mass transport rates at the interfaces between zones. The model is used to analyze the results of two sets of uptake experiments conducted on red spruce (13, 14). Sensitivity of the model to various measured and assumed parameters is examined.

II. Spruce Needle Physiology

Red spruce (*Picea rubens* Sarg.) needles are spirally set on the tree's branches (15). The needles are 10–15 mm in length and four-sided. The cross-section is roughly diamond-shaped (16, 17). The sides of the needles are 0.5–1.0 mm in width. Stomata are located in rows, two to four rows on a side, on all four sides of the needles (18). On Sitka spruce, the rows are spaced about 70 μm apart (19). Within stomatal rows, the distance between stomatal centers is reportedly 100 μm for Sitka spruce (19) and for leaves in general (20).

Figure 1 illustrates our idealization of the stomatal zone and includes our best estimates of appropriate dimensions, based on information found in the literature on a variety of spruce. The needles are covered with a relatively thick layer of wax so that the stomata appear to be sunken (16). The stomata are located below the V-shaped stomatal antechamber. The distance from the top of the antechamber to the mouth of the stomatal pore is roughly 18 μm (19). On Sitka spruce (19) and red spruce (21), this antechamber is filled with a wax plug, from the top of the guard cells nearly to the epidermal surface. On Sitka spruce, the depth of the plug is 15–18 μm (19). The wax is in the form of finely divided tubes 1 μm in length by 150

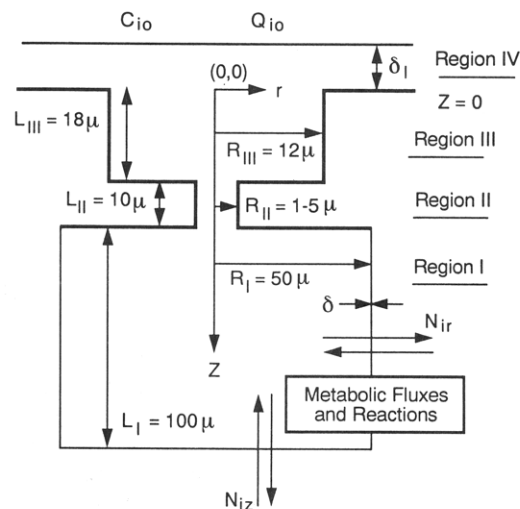


Figure 2. Schematic of red spruce stomatal zone, simplified for model. Transport is from the air–surface boundary (at $z = 0$) and directed inward. Concentrations (C_b) and fluxes (Q_b) of each species are known for the bulk air surrounding the needle. Region IV is the laminar boundary layer above the needle. Region III is the wax-filled stomatal antechamber, characterized as a porous medium filled with finely divided wax rodlets of length 1 μm and diameter 150 nm. The stomata is denoted as region II and is of varying radius, depending on whether nighttime or daytime conditions are assumed. The bottom and side boundaries surrounding the air-filled substomatal cavity, region I, are assumed to be a thin film of water of thickness approximately 1 μm or roughly that of the cell wall. All reactions of reactive trace gases are assumed to occur in this thin film of water. All fluxes of metabolic species (CO_2 , O_2 , and H_2O) are assumed to be evenly distributed throughout the water film. Radii for regions I–IV are denoted by R_i , etc. Heights of each region are denoted by L_i , etc. Cylindrical coordinates are assumed.

nm in diameter, and voids between the wax tubes are roughly 1–2 μm across (19). The wax is comprised of cutin, a polymeric material consisting mainly of the esters of 16- and 18-carbon carboxylic acids and containing two or three hydroxyl groups (20). The stomatal pore depth of Sitka spruce is approximately 6 μm (19). In general, the stomatal pore is elliptical in shape, and the distance across is usually 5–10 μm (20).

In the internal regions of the needle, the cell is surrounded by the cell wall which is comprised primarily of water (up to 90%) (22). Also found in the cell wall are enzymes such as peroxidase (23, 24), and other chemical species such as ascorbic acid (25), an antioxidant that may play an important role as an atmospheric photochemical oxidant scavenger (26). The cell wall is approximately 1 μm in thickness (22).

III. Mathematical Formulation

Figure 2 illustrates a simplified schematic diagram of the stomatal zone, depicting four regions. Region I is the substomatal chamber. Diffusion of species involved in metabolic processes and chemical reactions of reactive gases (such as the reaction of O_3 with ascorbic acid dissolved in the cell wall water) are assumed to occur only at these walls, which are assumed to be comprised mainly of water. The reactions of ozone with several hydrocarbon constituents present in cell material have been discussed by Tingey and Taylor (27) and by Chameides (26), who examined the relative loss rates of ozone through reaction with ascorbic acid and certain hydrocarbons and found that the rate of loss due to reaction with ascorbic acid was

the fastest. For lack of other available information, we therefore consider reaction with ascorbic acid for describing the ozone chemistry inside the needle. Transport through region II, the stomatal pore, is similar to flow through a small capillary. The pore radius is variable, depending primarily on light availability. The stomatal antechamber, region III, behaves as a porous medium packed with cylinders, through which diffusion is hindered by the tortuosity and porosity of the media. The uppermost region (region IV) is the laminar boundary layer over the needle surface. The thickness of this region, δ_1 , is a function of the velocity and turbulence of the bulk air above the leaf.

In the following analysis, cylindrical coordinates are assumed, and seven gaseous species are included. During photosynthesis, the plant takes up CO_2 and gives off O_2 . Because the inner plant tissues are largely made up of water, the inner air spaces have a high relative humidity (RH), and the plant gives off H_2O . Since there are concentration gradients for these species, there will be a concentration gradient in N_2 as well; therefore, this species is also considered, although we assume that there is no net flux of N_2 . The reactive trace gases under study are O_3 , SO_2 , and H_2O_2 .

Point Equations. Inside the substomatal chamber, the stomatal pore, and the antechamber (regions I–III), the governing equations for gas transport are the point continuity equations for each gaseous species i . Concentration gradients in the angular direction have been neglected. Quasi-steady-state conditions are assumed. All chemical reactions are assumed to be heterogeneous and to occur at the substomatal chamber wall only. With these assumptions, the continuity equation in cylindrical coordinates becomes

$$\frac{1}{r} \frac{\partial}{\partial r}(rN_{ir}) + \frac{\partial N_{iz}}{\partial z} = 0 \quad (3)$$

where N_i is the total molar flux of i relative to stationary coordinates. This flux results from both diffusive mechanisms and from bulk movement of gases

$$N_i = N_i^D + N_i^V \quad (4)$$

where the superscripts D and V denote “diffusive” and “viscous” (convective) contributions, respectively (10, 11), and boldface parameters denote vector quantities. The convective flux arises from a pressure gradient and corresponds to gas transport due to bulk movement of material

$$N_i^V = x_i N^V \quad (5)$$

where N^V is the total molar convective flux. Multicomponent diffusion for a mixture of n gases is described by the generalized form of the Stefan–Maxwell eq (28) for ideal solutions. We assume the gas mixture is isothermal and neglect the forced diffusion terms and the pressure diffusion term since the pressure gradient is expected to be slight. The modified form of the Stefan–Maxwell equation which includes Knudsen diffusion is used, extended to include vector quantities (10–12, 29)

$$-\frac{1}{RT} \nabla P_i = \frac{N_i^D}{D_{ii}^K} + \sum_{j=1, j \neq i}^n \frac{x_j N_j^D - x_i N_j^D}{D_{ij}} \quad (6)$$

where n is the number of species, ∇P_i , the gradient of the

partial pressure of i , is an expression of the concentration gradient of species i , R is the gas constant, T is the absolute temperature, D_{ii}^K is the Knudsen diffusivity of i , and the D_{ij} 's are the binary diffusion coefficients that are assumed to approximate the concentration-dependent multicomponent diffusivities at the low gas densities encountered in this problem (30).

Spatially Averaged Equations. In order to solve these equations, the technique of spatial averaging is applied. This allows us to treat the model as if it is one-dimensional, in that the concentrations and fluxes vary in the axial direction. We recognize, however, that stomatal transport is three-dimensional. By spatial averaging, we can take into account area changes in the direction of the flow that are due, for example, to fluxes at the wall.

Region I. The transport equations for region I are area-averaged in the radial direction. For this approximation to be valid, the concentration gradient in the radial direction should be much less than that in the axial direction. This criterion is met if the condition

$$\left(\frac{r_0}{L_0}\right)^2 \ll 1 \quad (7)$$

is satisfied, where r_0 and L_0 represent the radius and length of a given transport zone. In region I, this ratio has a value of 0.25, which is sufficiently small to justify this approach (31). The area-averaged form (28) of eq 3 for region I becomes

$$\frac{2}{R_1} N_{ir|r=R_1} + \frac{d}{dz} \langle N_{iz} \rangle = 0 \quad (8)$$

where $\langle N_{iz} \rangle$ represents the area-averaged flux of species i in the z direction, $N_{ir|r=R_1}$ is the flux at the wall, and r_1 is the radius of the substomatal region.

The Stefan–Maxwell equation must also be area-averaged, which results in dispersion terms that depend on second derivatives of the concentration gradient (Table I). These dispersion terms are neglected; therefore, the area-averaged Stefan–Maxwell equation takes the form

$$-\frac{1}{RT} \frac{\partial \langle P_i \rangle}{\partial z} = \frac{\langle N_{iz}^D \rangle}{D_{ii}^K} + \sum_{j=1, j \neq i}^n \frac{\langle x_j \rangle \langle N_{iz}^D \rangle - \langle x_i \rangle \langle N_{jz}^D \rangle}{D_{ij}} \quad (9)$$

The binary diffusivities for each gas are calculated from a Gilliland-type correlation (32). The Knudsen diffusivity for diffusion in a cylindrical tube of diameter d is calculated by (12, 32)

$$D_{ii}^K = \frac{d}{3} \left(\frac{8RT}{\pi M_i} \right)^{1/2} \quad (10)$$

where M_i is the molecular weight of species i . In pores or in porous media, Knudsen diffusion is expected to be insignificant when the pore size, d , is much larger than the molecular mean free path, λ , or when the Knudsen number, defined by (11)

$$K_n = \lambda/d \quad (11)$$

is much less than 1. The molecular mean free path is a function of temperature, pressure, and the molecular size (11)

$$\lambda = \frac{kT}{\sqrt{2} \pi \sigma^2 P} \quad (12)$$

Table I. Summary of Equations and Boundary Conditions Used in Model for Substomatal Chamber

region I	equation	comments
Stefan-Maxwell	$\frac{d\langle x_i \rangle}{dz} = \sum_{j=1, j \neq i}^n \frac{\langle x_i \rangle \langle N_{jz}^D \rangle - \langle x_j \rangle \langle N_{iz}^D \rangle}{cD_{ij}}$	(n - 1) equations
momentum eq	$\frac{d\langle P \rangle}{dz} = 0$	nth equation
continuity eq	$\frac{d\langle N_{iz} \rangle}{dz} = -\frac{2}{R_1} N_{i r=R_1}$	n equations
fluxes	$\langle N_{iz} \rangle = \langle N_{iz}^D \rangle$	
boundary conditions	$\langle N_i A \rangle_I = \langle N_i A \rangle_{II}$ $\langle P_I \rangle = \langle P_{II} \rangle$ $N_{i r=R_1} = 0$	mass conservation across interface $i = N_2$
miscellaneous parameters	$N_{i r=R_1} = \frac{Q_i(A_L)}{n_{st}(\pi R_1^2 + 2\pi R_1 L_1)}$	$i = O_2, CO_2, H_2O$
	$N_{i r=R_1} = kH \langle P_i \rangle \delta$	$i = SO_2, O_3, H_2O_2$
	$H_{O_3} \sim 10^{-2} \text{ mol L}^{-1} \text{ atm}^{-1}$	ref 26
	$H_{H_2O_2} \sim 10^5 \text{ mol L}^{-1} \text{ atm}^{-1}$	ref 35
	$H_{SO_2} \sim 10^0 \text{ mol L}^{-1} \text{ atm}^{-1}$	ref 36
	$k'_{O_3} \sim 10^4 \text{ s}^{-1}$	ref 26
	$k'_{SO_2} \sim 10^4 \text{ s}^{-1}$	estimated from k'_{O_3}
	$k'_{H_2O_2} \sim 10^4 \text{ s}^{-1}$	estimated from k'_{O_3}

where k is the Boltzmann constant and σ is the molecular radius. For N_2 at 20 °C and 10^5 Pa, $\lambda \approx 0.07 \mu\text{m}$ (12). The Knudsen number for N_2 in the substomatal region, then, is on the order of $K_n \approx 0.07/100$ so that in region I Knudsen diffusion may be neglected. Because the chamber is relatively large and open, no pressure gradients are expected in this region. The air inside the substomatal chamber is also assumed to be isothermal. The multi-component diffusion of the gas mixture at low density in region I can then be described by the Stefan-Maxwell equations (neglecting the Knudsen diffusion)

$$c \frac{d\langle x_i \rangle}{dz} = \sum_{j=1, j \neq i}^n \frac{1}{D_{ij}} (\langle x_i \rangle \langle N_{jz}^D \rangle - \langle x_j \rangle \langle N_{iz}^D \rangle) \quad (13)$$

where c is the total molar concentration or $\langle P \rangle / RT$. In this form, the Stefan-Maxwell equations result in (n - 1) independent equations. The n th equation is obtained from the momentum balance (10). Based on the assumption that the substomatal chamber is relatively isobaric compared to the stomatal pore, the n th equation becomes

$$\frac{d\langle P \rangle}{dz} = 0 \quad (14)$$

The surfaces of the guard cells are assumed to be inert. All other walls of the substomatal chamber are assumed to be composed mainly of water and are, therefore, treated as a liquid film of thickness δ ; therefore, the only source or sink of any gaseous species is through this film. Since we are primarily interested in the reactive air pollutants, for the unreactive gases (i.e., O_2 , CO_2 , and H_2O), the flux at the wall is assumed to be uniform for all surfaces. For a more detailed model of CO_2 assimilation, the kinetics of photosynthesis could also be included (e.g., ref 34). By material balance, the flux at this wall is related to the flux on a leaf area basis through the ratio of total leaf area to total internal surface area

$$N_{i|r=R_1} = \frac{Q(A_L)}{n_{st}A_{int}} \quad (15)$$

where Q is the experimentally determined molar flux to the leaves, A_L is the experimentally measured total leaf area, n_{st} is the number of stomata per unit leaf area, and

A_{int} is the reactive portion of the substomatal chamber wall surface area (i.e., the area of the liquid film) for a single substomatal cavity.

By mass balance, the flux of any reactive species at the cell wall can be related to the homogeneous reaction rate of consumption (R) in the liquid film on the surface of the cell wall

$$N_{i|r=R_1} = R\delta \quad (16)$$

where δ is the liquid film thickness. For O_3 , which is assumed to react with ascorbic acid in the cell wall (second-order-reaction rate constant is k), the water solubility is low (Henry's law constant $\approx 10^{-2} \text{ mol l}^{-1} \text{ atm}^{-1}$, 26). The concentration of ascorbic acid in the cell wall water ([AA]) is therefore not expected to change significantly, and the reaction expression is treated as a pseudo-first-order reaction

$$R_{O_3} = -k'_{O_3} H_{O_3} \langle P_{O_3} \rangle \quad (17)$$

where k'_{O_3} equals $k[AA]$ and is estimated to be on the order of $3000\text{--}60\,000 \text{ s}^{-1}$ (26). In this rate equation R_{O_3} is the rate of disappearance of O_3 in the cell wall by reaction, $\langle P_{O_3} \rangle$ is the partial pressure of O_3 in the substomatal chamber, and H_{O_3} is the Henry's law constant for O_3 ($\text{mol L}^{-1} \text{ atm}^{-1}$). For H_2O_2 and SO_2 the Henry's law constants are on the order of $10^5 \text{ mol L}^{-1} \text{ atm}^{-1}$ (35) and $10^0 \text{ mol L}^{-1} \text{ atm}^{-1}$ (ref 36, and references cited therein), respectively. The pseudo-first-order rate constants for the reactions of H_2O_2 and of SO_2 in the cell wall water are assumed to be similar to that given above for O_3 .

Region II. In the stomatal pore (region II), the pore radius to length ratio ranges from 0.05:10 or less to 5:10, depending on whether the stomata are closed or open. Therefore, according to the criterion of eq 7, it is adequate to area-average the governing equations for this region as well. The area-averaged form of the continuity equation (eq 8) and the area-averaged form of the Stefan-Maxwell equation (eq 9) are applied to gas transport in this region. Because of the small dimensions of the stomatal pore, the Knudsen number ranges from 0.01 to 0.1 in the stomata. Both Knudsen and molecular diffusion could therefore contribute to the gas transport in region II. The Knudsen

Table II. Summary of Equations and Boundary Conditions Used in Model for Stomatal Pore

region II	equation	comments
Stefan-Maxwell	$-\frac{1}{RT} \frac{d\langle P_i \rangle}{dz} = \frac{\langle N_{iz}^D \rangle}{D_{ii}^K} + \sum_{j=1, j \neq i}^n \frac{\langle x_j \rangle \langle N_{jz}^D \rangle - \langle x_i \rangle \langle N_{iz}^D \rangle}{D_{ij}}$	(n - 1) equations
	$-\frac{1}{RT} \frac{d\langle P \rangle}{dz} = \sum_{i=1}^n \frac{\langle N_{iz}^D \rangle}{D_{ii}^K}$	nth equation
convective flux	$\langle N_z^V \rangle = -\frac{(2R_{II})^2 \langle P \rangle}{32\mu} \frac{d\langle P \rangle}{RT dz}$	
continuity	$\frac{d\langle N_{iz} \rangle}{dz} = -\frac{2}{R_{II}} N_{iz} _{r=R_{II}}$	n equations
boundary conditions	$\begin{aligned} \langle \langle N_{iz} \rangle A \rangle_{II} &= \langle \langle N_{iz} \rangle A \rangle_{III} \\ \langle P_{II} \rangle &= \langle P_{III} \rangle \\ N_{iz} _{r=R_{II}} &= 0 \end{aligned}$	conservation of mass across interface $i = \text{CO}_2, \text{H}_2\text{O}, \text{O}_2, \text{N}_2, \text{SO}_2, \text{O}_3, \text{H}_2\text{O}_2$

diffusion term is therefore retained in the Stefan-Maxwell equation for region II (Table II).

In region II, both diffusive and convective fluxes contribute to the total flux. The convective flux in the stomata is assumed to behave similarly to that in a capillary tube, and the Hagen-Poiseuille equation for laminar flow of gases in capillaries (11, 30) can be assumed to be valid

$$\langle N_z^V \rangle = -\frac{(2R_{II})^2 \langle P \rangle}{32\mu} \frac{\partial \langle P \rangle}{RT \partial z} \quad (18)$$

where μ is the gas viscosity, and R_{II} is the stomatal radius.

The *n*th equation is, again, an expression of the momentum balance and can be obtained by writing the modified Stefan-Maxwell equation for the total pressure, making use of the relationship $\langle P \rangle = \sum_{i=1}^n \langle P_i \rangle$. Because of the constraint on the diffusive fluxes that they sum to zero, the resulting expression for the *n*th equation becomes

$$-\frac{1}{RT} \frac{\partial \langle P \rangle}{\partial z} = \sum_{i=1}^n \frac{\langle N_{iz}^D \rangle}{D_{ii}^K} \quad (19)$$

The walls of the stomatal pore are assumed to be impermeable and nonreactive; therefore, in region II the wall boundary condition is zero for all species

$$N_{iz}|_{r=R_{II}} = 0 \quad (20)$$

Region III. The antechamber (region III) is filled with finely divided wax tubes and behaves as a porous medium. In this region, the equations are volume-averaged, using the spatial averaging theorem (28). Ignoring dispersion terms and any potential losses due to absorption on surfaces in this region, the volume-averaged form of the continuity equations becomes

$$\frac{d}{dz} \langle N_{iz} \rangle = 0 \quad (21)$$

for gaseous species *i* which do not react with the surfaces in this region. This region is thought to be relatively inert to SO₂ and O₃ and reactive to H₂O₂. Although it is recognized that reactive gases may be lost due to heterogeneous reaction in this region, for the remainder of these calculations the reaction rates for O₃, H₂O₂, and SO₂ are assumed to be zero so that the concentration profiles calculated represent upper limits.

Similarly, the Stefan-Maxwell equation must be volume-averaged. Applying volume-averaging and again neglecting dispersion terms, the *z*-component of the Stefan-

Maxwell equation becomes

$$-\frac{1}{RT} \frac{\partial \langle P_i \rangle}{\partial z} (1 + \phi) = \frac{\langle N_{iz}^D \rangle}{D_{ii}^K} + \sum_{j=1, j \neq i}^n \frac{\langle x_j \rangle \langle N_{jz}^D \rangle - \langle x_i \rangle \langle N_{iz}^D \rangle}{D_{ij}} \quad (22)$$

where ϕ is the component of the tortuosity tensor along the *z*-direction (37).

The effective diffusivities can then be written in terms of the diffusion coefficients and the correction factor (1 + ϕ) that is related to the volume fraction ϵ (the porosity, or the ratio of pore volume to total volume) and the tortuosity τ of the porous medium

$$D_{ij, \text{eff}} = D_{ij}(1 + \phi) = \frac{\epsilon}{\tau} D_{ij} \quad (23)$$

and the volume-averaged Stefan-Maxwell equation in the *z*-direction becomes (Table III)

$$-\frac{1}{RT} \frac{\partial \langle P_i \rangle}{\partial z} = \frac{\langle N_{iz}^D \rangle}{D_{ii, \text{eff}}^K} + \sum_{j=1, j \neq i}^n \frac{\langle x_j \rangle \langle N_{jz}^D \rangle - \langle x_i \rangle \langle N_{iz}^D \rangle}{D_{ij, \text{eff}}} \quad (24)$$

In region III, the void spaces in the porous media are very small so that both molecular and Knudsen diffusion are considered to be important. The Knudsen number in this region is on the order of 0.1-1.0. The total flux includes both diffusive and convective contributions. The convective flux is described by Darcy's law for flow through a porous medium (11, 28, 30)

$$\langle N_z^V \rangle = -c \frac{k_p}{\mu} \frac{\partial \langle P \rangle}{\partial z} \quad (25)$$

where *c* is the total concentration of gases. The permeability, *k_p*, can be estimated by the laminar contribution to the Ergun equation (30)

$$k_p = \frac{d_p^2 \epsilon^3}{150(1 - \epsilon)^2} \quad (26)$$

where *d_p* is the characteristic particle length.

Region IV. The total flux of species *i* in the *z*-direction through the boundary layer is assumed to include contributions from both the diffusive flux and the bulk convective flow (12, 30). The diffusive component is proportional to the concentration gradient

$$N_{iz}^D = -k_{im} \Delta x_{ib} \quad (27)$$

where *k_{im}* is the boundary layer mass-transfer coefficient

Table III. Summary of Equations Used in Model for Porous Antechamber

region III	equation	comments
Stefan-Maxwell	$-\frac{1}{RT} \frac{d\langle P_i \rangle}{dz} = \frac{\langle N_{iz}^D \rangle}{D_{ii,eff}^K} + \sum_{j=1, \neq i}^n \frac{\langle x_i \rangle \langle N_{jz}^D \rangle - \langle x_j \rangle \langle N_{iz}^D \rangle}{D_{ij,eff}}$	(n - 1) equations
	$-\frac{1}{RT} \frac{d\langle P \rangle}{dz} = \sum_{i=1}^n \frac{N_i^D}{D_{ii,eff}^K}$	nth equation
continuity	$\frac{d\langle N_{iz} \rangle}{dz} = 0$	n equations
fluxes	$\langle N_{iz}^D \rangle = \langle N_{iz} \rangle - x_i \langle N_z^Y \rangle$ $N_z^Y = -c \frac{k_p}{\mu} \frac{d\langle P \rangle}{dz}$ $k_p = \frac{d_p^2 \epsilon^3}{150(1 - \epsilon)^2}$ $D_{ii,eff}^K = D_{ii}^K Q_p$ $D_{ij,eff}^K = D_{ij}^K Q_p$ $Q_p = \epsilon / \tau$	
boundary conditions	$\langle (N_{iz}) \rangle_{III} = \langle (N_{iz}) \rangle_{IV}$ $P_{III} = P_{IV}$	conservation of mass across interface

Table IV. Summary of Equations and Boundary Conditions Used in Model for Boundary Layer

region IV	equation	comments
	$x_{io} = \frac{-N_{iz} + x_{ib}(k_{im} + 1/2N_z)}{k_{im} - 1/2N_z}$	n equations
fluxes	$N_z = \sum_{j=1, \neq i}^n N_{jz}$ $k_{im} = J_D \nu (Sc_i)^{-2/3}$ $J_D = 0.600(Re)^{-0.487}$ $Sc_i = \frac{\mu}{\rho D_i}$ $Re = \frac{\nu D_p}{\mu}$	
boundary conditions	$\langle N_{iz} \rangle_{IV} = Q_i$	initial conditions
x_{ib}	ambient mole fraction of i	measured experimentally
Q_i	molar flux of i per unit leaf area	measured experimentally
ν	air velocity near needles	measured experimentally

for species i , Δx_{ib} is a characteristic concentration gradient between the leaf surface/air interface (x_{io}) and the bulk ambient concentration above the leaf (x_{ia}). The convective component of the flux is given by

$$N_{iz}^Y = \langle x_{ib} \rangle \sum_{j=1, \neq i}^n N_{jz} \quad (28)$$

where $\langle x_{ib} \rangle$ is the characteristic mean concentration of the boundary layer. If we assume that $\langle x_{ib} \rangle = (x_{ia} + x_{io})/2$ and that $\Delta x_{ib} = x_{io} - x_{ia}$, then we can solve for the concentration at the top of the leaf surface (12)

$$x_{io} = \frac{-N_{iz} + x_{ib}(k_{im} + 1/2N_z)}{k_{im} - 1/2N_z} \quad (29)$$

where N_z is the total molar flux in the z -direction (Table IV). The mass-transfer coefficient can be correlated to the Colburn j factor (J_D) (30), a dimensionless parameter which is, in turn, related to the Schmidt number, Sc_i ,

$$J_D = \frac{k_{im}}{\nu} (Sc_i)^{2/3} \quad (30)$$

For O_3 diffusion in air at 25 °C and 1 atm, the Schmidt

number is 0.78. The dimensionless parameter, J_D , is empirically correlated for a number of geometries. For gaseous flow past single cylinders, J_D is correlated to the Reynolds number, Re (38)

$$J_D = 0.600(Re)^{-0.487} \quad (31)$$

This correlation applies for cylinders for which mass transfer to the ends is not considered, for Schmidt numbers ranging from 0.6 to 2.6 for gases, and for Reynolds numbers of 50–50 000. The characteristic length used in the calculation of Re is the cylinder diameter. For a wind speed of 30 cm s⁻¹, needle diameter of 1 mm, and air at 25 °C and 1 atm, the Reynolds number is 20.

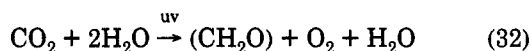
Boundary Conditions and Computational Methods.

Summaries of all equations for each region are given in Tables I–IV. To formulate this problem, for each region a set of nonlinear, ordinary differential equations is solved. The boundary conditions for each region include the flux at the wall and the flux in the axial direction at the top of each section. Since we only know the fluxes and concentrations at the outer surface of the leaf, we start at the boundary layer and work inward. The fluxes and concentrations calculated at the end of one region are used then as the initial boundary conditions for the next region.

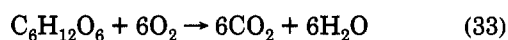
Since this problem is set up as an initial value problem, and since the formulation includes a series of nonlinear, ordinary differential equations, the Runge–Kutta method is used to solve the problem in a stepwise fashion through the leaf, starting at the ambient air interface. Conservation of mass and continuity of pressure are assumed at each interface. Given a constant mass rate across the boundary between regions, the concentration is calculated across the interface and at each step. If, at any point during the calculation, the concentration of a given species is calculated to be less than zero, it is set equal to zero, and the entire set of equations is reduced by also setting the flux of the species and the derivatives of both the concentration and the flux of that species to zero.

The fluxes of CO_2 , H_2O , O_3 , SO_2 , and H_2O_2 as determined from controlled environment chamber tests and the atmospheric concentrations of all species provide initial conditions. We assume that the net flux of N_2 is zero. To estimate the O_2 flux, we consider relevant plant processes. During photosynthesis, CO_2 and H_2O are metabolized to

synthesize carbohydrates (39)



During respiration (which occurs during both day and night), glucose and other carbohydrates are oxidized to produce CO_2 and water (39)



Based on these chemical processes then, we assume that the net flux of O_2 is equal in magnitude but opposite in direction to the net flux of CO_2 , for both daytime and nighttime cases. Water vapor evolved as a product of photosynthesis and respiration is neglected in the following analysis because its contribution to the total transpiration rate is very small. The relative humidity in the intercellular spaces is generally thought to be between 96 and 99% (40); the relative humidity in the substomatal chamber is therefore assumed to be 98.5% in the following analysis. Since the substomatal H_2O concentration is calculated in this procedure, the resulting relative humidity is compared to 98.5%, the stomatal radius is adjusted, and the entire calculation is repeated until this criterion is satisfied.

IV. Results and Discussion

Two sets of experiments were analyzed using this model. The first set investigated the simultaneous exposure of isolated branches of red spruce to a combination of O_3 , SO_2 , and H_2O_2 (13). The second set of experiments, presented in a companion paper (14), measured the uptake rate of gaseous H_2O_2 by red spruce saplings in a whole-tree, continuous mixed-flow exposure chamber (MFC).

Simultaneous Exposure of SO_2 , O_3 , and H_2O_2 . Base Case: Ennis et al. (13) Daytime Conditions. A summary of the operating parameters used to establish a base case (from ref 13) is given in Table V. The stomatal radius is assumed to be $2.5 \mu\text{m}$ for daytime conditions. The stomatal density (per cm^2) was adjusted until the desired relative humidity in the substomatal chamber (region I) was 98.5%. For the base case, we estimated 2850 stomata per cm^2 of leaf area. Jeffrey et al. (14) have suggested a stomatal density as high as 6000 per cm^2 for greenhouse-grown spruce.

Concentration profiles for CO_2 , H_2O , and O_3 , SO_2 , and H_2O_2 are shown in Figures 3–5. The base case substomatal CO_2 concentration calculated by the model is approximately 148 ppm. This value is comparable to or lower than values reported elsewhere that were estimated for spruce using a multiple resistance method. Estimates have ranged from approximately 170 to 200 ppm for Sitka spruce (41) and from 50 to 270 ppm for several coniferous species for a range of water and ambient CO_2 conditions (42).

From Figures 3–5 and Table VI we see that, during the daytime, the stomatal antechamber (region III) provides an important resistance to gas transport. It also appears that there is a significant sink in this region for H_2O_2 and SO_2 , which disappear shortly after entering this porous zone. The O_3 concentration appears to approach zero in or near the stomatal pore, which is consistent with both experimental and mathematical results reported by other researchers. Laisk et al. (43) concluded that the O_3 concentration in the leaf intercellular air space is nearly zero based on chamber uptake experiments on sunflowers. Chameides (26) calculated that, for cell wall thickness of

Table V. Input Parameters for Base Case^a

parameter	daytime	nighttime
Concentrations		
[CO_2], ppm	353.7	353.0
[H_2O], ppth	22.58	20.68
[O_3], ppb	88.6	92.1
[H_2O_2], ppb	3.3	3.9
[SO_2], ppb	10.4	8.6
Fluxes, $\text{mol m}^{-2} \text{s}^{-1}$		
CO_2	$1.09 (10^{-6})$	$-0.194 (10^{-6})$
H_2O	$-1.49 (10^{-4})$	$-0.162 (10^{-4})$
O_3	$8.58 (10^{-10})$	$4.41 (10^{-10})$
H_2O_2	$2.85 (10^{-10})$	$4.23 (10^{-10})$
SO_2	$3.97 (10^{-10})$	$4.20 (10^{-10})$
Chamber Conditions		
T , °C	26.0	20.5
P , atm	0.815	0.815
RH, %	56.0	71.4
v , cm s^{-1}	30.0	30.0
Assumptions		
VPD, ppth	17.7	8.3
n_{st} , cm^{-2}	2850	2850
ϵ/τ	0.5/3	0.5/3

^a Base case conditions taken from ref 13. Concentrations are those measured at the outlet of the enclosed branch chamber. Fluxes are per unit area of leaf area as measured by a glass bead technique. v is the air velocity next to the needle. To run the simulation, the leaf temperature was assumed to be that of the chamber and the inner water vapor content was determined by assuming 98.5% relative humidity in the substomatal cavity. VPD is the vapor pressure deficit across the stomata (ppth), or the difference between the water vapor content of the air next to the needle and the water vapor content in the substomatal cavity (i.e., the intercellular water vapor content). The stomatal number density is assumed to be 2850 per cm^2 of needle surface area. The ratio ϵ/τ is the obstruction factor assumed for the stomatal antechamber.

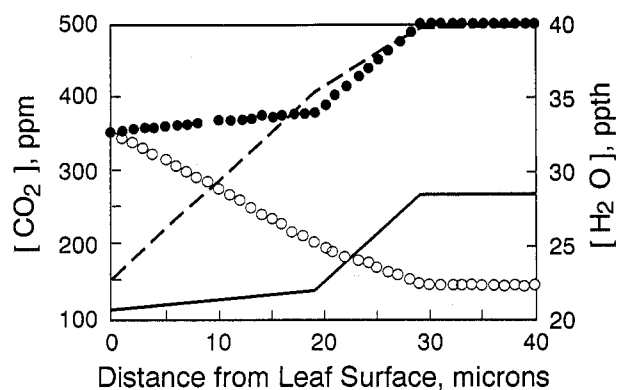


Figure 3. Concentration profiles for CO_2 , water vapor, in stomatal zone. These profiles are for idealized stomatal zone in red spruce needle and are the results of the simulation of the base case taken from ref 13. Daytime and nighttime CO_2 profiles are indicated by open and filled circles, respectively. Daytime and nighttime H_2O profiles are indicated by dashed and solid lines, respectively. Intercellular CO_2 concentration is approximately 150 ppm for the daytime case and approximately 500 ppm for the nighttime case. This figure illustrates that the porous antechamber ($z = 0$ to $z = 18 \mu\text{m}$) provides a significant resistance to gas transport, particularly during the daytime, while at night the stomata ($z = 18$ to $z = 28$) contributes a larger resistance.

on the order of a few tenths to $10 \mu\text{m}$, the fraction of O_3 molecules reacting with ascorbic acid may approach 1, suggesting that it may be possible that most of the O_3 diffusing into the intercellular region reacts immediately.

Case II: Nighttime. Most plant species, including spruce, partially close their stomata at night, probably in response to an increasing internal CO_2 concentration,

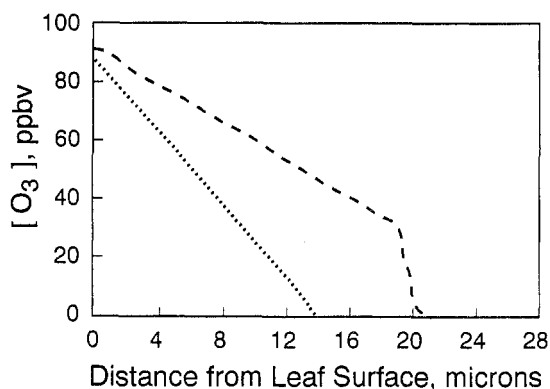


Figure 4. Concentration profiles for reactive trace gas O_3 in stomatal zone. Daytime and nighttime profiles are indicated by dotted and dashed lines, respectively. Concentration profiles are for idealized stomatal zone of red spruce and are the results of simulation of base taken from ref 13.

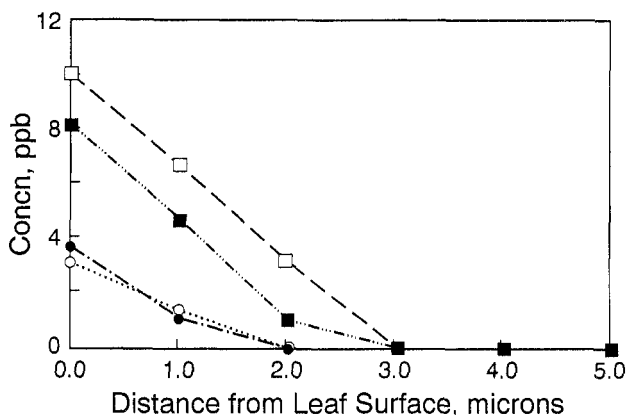


Figure 5. Concentration profiles for reactive trace gases SO_2 and H_2O_2 in stomatal zone. SO_2 daytime and nighttime profiles are denoted by filled and open squares, respectively. H_2O_2 daytime and nighttime profiles are denoted by filled and open circles, respectively. Concentration profiles are for idealized stomatal zone of red spruce and are the results of simulation of base case taken from Ennis *et al.* (13). This figure indicates that both H_2O_2 and SO_2 disappeared in the stomatal antechamber, well before reaching the stomata.

which occurs as light available for photosynthesis is reduced (44, 45). Therefore, to simulate case II (nighttime), the stomatal pore radius was reduced from 2.5 to 0.92 μm in order to maintain the relative humidity in the substomatal zone, which is assumed to remain roughly constant inside the plant needle, again at approximately 98.5%. Due primarily to this reduction in stomatal aperture, we find that now the stomatal pore itself provides a very significant resistance to gas exchange (Figures 3–5; Table VI). Similar to the daytime case, the trace species disappear before reaching the substomatal region.

H_2O_2 Uptake Experiments. The H_2O_2 uptake experiments conducted by Claiborn and Aneja (14) employed a whole-tree MFC containing 2–4 red spruce saplings. A series of experiments were conducted for varying dewpoint temperature and inlet H_2O_2 concentration. The CO_2 and H_2O fluxes were periodically calculated. The CO_2 concentration was 450 ± 50 ppm during the day and 390 ± 30 ppm at night. The average CO_2 flux was $(2.31 \pm 0.71) \times 10^{-9}$ mol cm^{-2} s^{-1} during the day and $-(1.54 \pm 0.83) \times 10^{-9}$ mol cm^{-2} s^{-1} at night. It should be pointed out that the levels of CO_2 exchange measured in the experiments of Claiborn and Aneja (14) are higher than those measured for red spruce by other investigators. Ennis *et al.* (13)

measured daytime exchange rates on the order of 10^{-10} mol cm^{-2} s^{-1} for a red spruce sapling in their branch chamber experiments. Hanson and McLaughlin (46) reported similar rates for red spruce seedlings. Pier *et al.* (47) and McLaughlin *et al.* (48) reported rates of approximately 0.05 and 0.055 μmol s^{-1} per g of dry weight for red spruce seedlings in field exclusion chambers and red spruce saplings in their natural environment, respectively. Using a ratio of 1.5 g of dry weight per 200 cm^2 leaf area (13), these rates correspond to 4×10^{-10} mol cm^{-2} s^{-1} , which is somewhat higher than those rates measured by Ennis *et al.* (13) and Hanson and McLaughlin (46), but not as high as those measured by Claiborn and Aneja (14). These apparent discrepancies may be due to the elevated CO_2 condition of the latter experiments or to differences in leaf area measurement techniques. For simulating these experiments, the CO_2 concentration was assumed to be 400 ppm, and the flux was set at average values.

The H_2O flux for each experiment was correlated to the exposure chamber outlet water vapor pressure difference across the leaf (VPD) (Figure 6). In order to compute the vapor pressure difference, the leaf temperature was assumed to be equal to the chamber air temperature. During periods for which the light was on (days), the temperature was 25.0 ± 1.0 $^{\circ}C$. At night (when the light was off) the temperature was 22.5 ± 1.0 $^{\circ}C$. As before, the inner (substomatal) relative humidity was assumed to be 98.5%. We calculated an error of approximately 35% associated with this method of estimating the water vapor flux.

The operating conditions for these experiments are summarized in Table VII. To model these experiments, the stomatal density calculated from the base case was retained, and the stomatal radius required to obtain 98.5% relative humidity was recalculated. With the exception of the first daytime run, the H_2O_2 disappears in approximately the same place for this set of experiments, or at approximately $z = 4$ – 6 μm for daytime runs (Table VIII). The previous simulations of the base case and case II indicated that the H_2O_2 disappeared earlier (at $z = 2$ μm). The results of the current simulations of the nighttime experiments were more variable than those for the daytime experiments for prediction of the location at which the H_2O_2 concentration goes to zero (at z between 2 and 10 μm). The reason for this variability is not known.

The stomatal radius calculated based on 2850 stomata per cm^2 was considerably lower than that assumed for the base case (0.9–1.5 μm compared to 2.5 μm). It is interesting to note that for the nighttime case the radii calculated were much more similar to that calculated in case II (0.9–1.2 μm compared to 0.9 μm). The stomatal radius responds to a number of factors including CO_2 concentration of the air. For example, when the CO_2 concentration in the air is increased, the stomata tend to close (44). This factor may have contributed to the difference in calculated radii, since the experiments by Claiborn and Aneja (14) were conducted at higher CO_2 concentration (400–500 ppm compared to 354 ppm). The CO_2 concentration would have less of an effect at night, so that the calculations for the nighttime conditions are consistent with this hypothesis. The stomatal pore size is also related to the VPD; many plants close their stomata as the relative humidity decreases (and the VPD increases) (44). For the series of experiments by Claiborn and Aneja, the relative humidity varied from 34 to 65% during the day and from 37 to 68%

Table VI. Results for Base Case^a

parameter	boundary layer	antechamber	stomata	substomatal chamber
		Daytime		
[CO ₂], ppm	353.1	218.5	148.7	147.9
[H ₂ O], ppth	22.64	33.97	39.73	39.80
RH, %	56.0	84.1	98.30	98.5
[O ₃], ppb	88.21	0, z = 14		
[H ₂ O ₂]		0, z = 2		
[SO ₂]		0, z = 3		
		Nighttime		
[CO ₂], ppm	353.1	377.5	498.2	499.1
[H ₂ O], ppth	20.69	21.99	28.43	28.48
RH, %	71.6	76.1	98.3	98.5
[O ₃], ppb	91.86	34.02	0, z = 21	
[H ₂ O ₂]		0, z = 2		
[SO ₂]		0, z = 3		
		Resistances, s mm ⁻¹		
overall r, H ₂ O, day	4.71			
overall r, CO ₂ , day	7.69			
for water vapor, day	0.016	3.10	1.58	0.019
for carbon dioxide, day	0.024	5.03	2.61	0.032
overall r, H ₂ O, night	19.98			
overall r, CO ₂ , night	31.26			
for water vapor, night	0.026	3.33	16.50	0.179
for carbon dioxide, night	0.021	5.23	25.81	0.208
stomatal radius, day, μm	2.5			
stomatal radius, night	0.92			

^a Concentrations are indicated for the bottom of each region as shown in Figure 2. The resistances are calculated from the relationship $Q = \Delta C/r$ where Q is the flux and ΔC is the concentration difference between the top and bottom of a given region. The leaf temperature is assumed to be equal to the air temperature, given in Table V. The stomatal radius is calculated assuming stomatal number density of 2850 per cm² of leaf area.

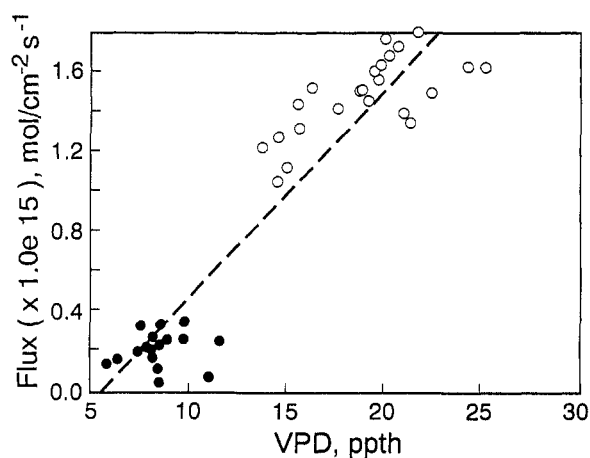


Figure 6. Correlation between water vapor flux and vapor pressure deficit. Water vapor flux to red spruce branches has units of mol cm⁻² s⁻¹. The vapor pressure deficit (VPD) is the difference between the chamber water vapor content and the water vapor concentration inside the substomatal cavity (assumed to be at 100% RH, at the air temperature in the chamber), ppth. Filled circles denote light-off (nighttime) conditions; open circles denote light-on. Flux ($\times 10^{15}$ mol cm⁻² s⁻¹) = 0.105 (VPD, ppth) - 0.582, $r^2 = 0.885$.

during the night (Table VII). The largest radius calculated for these experiments was 1.5 μm for 65% RH (run 6a). The experiments by Ennis et al. (13) were operated at a lower relative humidity (57%) during the day and (73%) at night.

Sensitivity Analysis. Leaf Temperature. In order to estimate the internal water vapor content, the leaf temperature was assumed to be equal to the ambient temperature. In reality, however, there may be a difference of several degrees between these temperatures. When the leaf temperature was varied in the base case from 26 to 29 °C (Table IX), the calculated substomatal CO₂ con-

Table VII. Experimental Conditions for Series of Uptake Measurements, Measuring Fluxes of Gaseous Hydrogen Peroxide to Red Spruce Saplings

sequence no.	run no.	[H ₂ O] ^a ppth	Q _{H₂O} ($\times 10^9$) mol cm ⁻² s ⁻¹	[H ₂ O ₂] ppb	Q _{H₂O₂} ($\times 10^{15}$) mol cm ⁻² s ⁻¹
Days					
1	3a	10.50	6.10	1.04	2.2
2	3b	11.46	5.81	0.06	2.6
3	3c	15.66	4.45	0.57	3.8
4	3d	15.10	4.32	2.08	9.9
5	4	13.79	4.00	1.51	7.2
6	5	15.25	5.19	1.33	6.2
7	6a	20.06	10.37	1.02	6.2
8	6b	18.06	11.37	1.46	7.0
11	7	15.57	3.26	2.52	13.6
13	9	18.57	6.02	2.60	12.4
Nights					
2	3b	9.77	2.60	0.18	1.9
3	3c	17.42	1.97	0.69	3.1
4	3d	17.42	1.97	2.10	7.6
5	4	13.24	2.20	2.22	7.4
7	5	13.24	2.81	1.05	5.8
11	7	17.93	2.56	2.71	11.6
13	9	17.93	4.10	3.53	14.2

^a [H₂O] and [H₂O₂] are the concentrations in the bulk air exiting the MFR chamber. Q_{H₂O}, Q_{H₂O₂} are the fluxes of water vapor and hydrogen peroxide, respectively, per cm² of leaf area. From ref 14.

centration changed from 148 to 48 ppm. The water vapor concentration, at constant 98.5% RH in the substomatal chamber, changed from 40 to 48 ppth (parts per thousand). The stomatal radius required to give 98.5% RH changed from 2.5 to 1.6 μm. The leaf temperature was found to be important when determining the intercellular CO₂ concentration and the stomatal radius; however, since the trace gases all disappeared before reaching the substomatal cavity, the leaf temperature had little effect on their concentration profiles.

Table VIII. Results of Simulations of Experiments of Claiborn and Aneja (14)^a

run no.	stomatal density	radius of stomata, μm	[CO ₂] ppm	[H ₂ O] ppth	VPD ppth	RH %	$z, \text{H}_2\text{O}_2 = 0 \mu\text{m}$
Days							
3a	2850	0.89	200.6	30.8	20.3	34.1	17
3b	2850	0.92	214.7	30.6	19.3	36.9	1
3c	2850	1.08	267.2	30.7	15.0	51.1	4
3d	2850	1.05	259.5	30.8	15.7	49.0	6
4	2850	1.00	244.9	30.5	16.7	45.2	6
5	2850	1.07	264.8	30.4	15.2	50.0	5
6a	2850	1.50	324.2	30.8	10.7	65.3	4
6b	2850	1.25	298.8	30.7	12.6	59.0	6
7	2850	1.29	304.1	30.8	15.2	50.6	5
9	2850	1.29	304.7	30.8	12.2	60.4	6
3a	900	2.5	259.3	30.8	20.3	34.1	6
6a	1750	2.5	443.0	30.4	10.3	66.1	3
Ennis <i>et al.</i>	2850	2.50	136.6	39.8	17.2	56.8	2
Nights							
3b	2850	0.87	525.1	26.5	16.7	37.0	2
3c	2850	1.20	464.5	26.3	8.9	66.0	7
3d	2850	1.19	465.5	26.5	9.0	66.0	9
4	2850	0.97	498.5	26.5	13.3	49.8	10
5	2850	0.97	498.5	26.5	13.3	49.8	6
7	2850	1.23	461.7	26.5	8.6	67.5	7
9	2850	1.23	461.7	26.5	8.6	67.5	8
Ennis <i>et al.</i>	2850	0.92	499.1	28.5	7.8	72.6	2

^a The stomatal density is that assumed, per cm² of leaf area, for each run simulation. The stomatal radius is that necessary to give 98.5% RH in the intercellular area (i.e., the substomatal chamber, region I). Calculations for experiments 3a and 6a were also repeated using a stomatal radius of 2.5 μm , and the stomatal density was adjusted to achieve 98.5% RH in the substomatal chamber [CO₂], and [H₂O] are the intercellular carbon dioxide and water vapor concentrations. VPD is the water vapor pressure difference between the bulk air and the intercellular air. RH is the bulk air relative humidity. The last column gives the location, as distance from the leaf surface, at which the hydrogen peroxide concentration is calculated to disappear.

Table IX. Sensitivity Studies^a

case	[CO ₂] _{int} , ppm	[H ₂ O] _{int} , ppth	$r_{st}, \mu\text{m}$	$z, \mu\text{m}$, for [H ₂ O ₂] = 0	$z, \mu\text{m}$, for [SO ₂] = 0	$z, \mu\text{m}$, for [O ₃] = 0
base case, day	147.9	39.8	2.5	2	3	14
night	499.1	28.5	0.92	2	3	21
$T_{leaf} + 3\text{C}$	47.5	48.1	1.64	2	3	14
$T_{leaf} - 1\text{C}$	172.1	37.8	3.20	2	3	14
$\tau = 2.0$	143.7	40.1	1.89	3	5	21
$\tau = 5.0$	146.6	40.0	7.0	2	3	11
$Q_i + 10\%$	148.4	39.8	3.00	2	3	13
$Q_i - 10\%$	147.8	39.8	2.17	2	4	16
$n_{st} + 50\%$ (4275)	146.7	39.8	1.63	3	5	21
$n_{st} - 20\%$ (2300)	149.4	39.8	4.50	2	3	12
$z_1 = 15$ and $z_2 = 5 \mu\text{m}$	147.7	39.8	1.64	2	3	14
$d_p = 1.5 \mu\text{m}$	147.1	39.8	1.99	3	4	20
$d_p = 0.75 \mu\text{m}$	149.2	39.8	4.7	2	3	11
0.75 flux	147.9	39.8	2.5	4	3	14
0.50 flux	147.9	39.8	2.5	8	3	14
0.25 flux	147.9	39.8	2.5	17	3	14

^a Base case conditions taken from average daytime (light-on) conditions given by ref 13. Nighttime case denotes light-off. Leaf temperature (T_{leaf}) in base case is assumed to be equal to chamber air temperature. τ is the estimated stomatal antechamber tortuosity (=3.0 in base case). Q_i denotes the chamber airflow rate, slpm. n_{st} is the assumed stomatal density (cm⁻¹), 2850 in base case. z_1 and z_2 are the distances from the air-leaf interface to the bottom of the antechamber, and bottom of stomata, respectively (assumed to be 18 and 28 μm , respectively). d_p is the assumed particle diameter, assumed to be 1.0 μm in base case. The flux in the last three rows refers to H₂O₂ and represents the fraction of the total flux to the vegetative surfaces to reach the stomatal zone, varied from 100% (base case) to 75%, 50%, and 25%.

Porous Plug Parameters. The effect of the ratio of bed porosity to tortuosity was examined since this value was assumed to be equal to average values for porous media. We found that the characteristics of the waxy plug had little effect on the calculated intercellular CO₂ concentration. This parameter was, however, important to the concentration profiles of the trace species in the wax plug (Table IX).

Gas Fluxes. The fluxes of all gases were determined from the total chamber airflow rate, the concentration difference across the reactor, and the leaf area. Therefore, errors in any of these measurements will affect the gas flux calculations. We varied the fluxes of all species by

$\pm 10\%$ and found that there was little impact on the CO₂ concentration profile and a small effect on the trace gas concentration profiles. For example, reducing the total airflow rate and gaseous fluxes changed the location at which the O₃ concentration disappears from 14 to 16 μm from the leaf surface.

Stomatal Density. In order to examine the sensitivity of this model to estimated stomatal number density, the stomatal density was decreased by 20%. In order to keep 98.5% RH inside the needle for this density, it was necessary to increase the stomatal pore radius to 4.5 μm . While the CO₂ concentration was not changed significantly as a result of these changes, the profiles of the traces gases

did respond to this parameter. The effect on the O₃ profile, in particular, was that the concentration approached zero at an earlier location in the stomata.

Stomatal Dimensions. Dimensions of the stomatal region were also adjusted to examine the effects on the model calculations. The wax plug depth (z_1) was adjusted from 18 to 15 μm , and the stomatal depth (z_2) was reduced from 10 to 5 μm , so that the top of the substomatal chamber was then located at $z = 20 \mu\text{m}$ rather than at $z = 28 \mu\text{m}$ in the base case. The resulting profiles indicate that the internal concentrations of H₂O and CO₂ do not change substantially; however, the point at which the O₃ concentration goes to zero is much closer to the top of the substomatal chamber.

The ozone concentration in the substomatal chamber appears to be zero for all the cases that were considered in this study. This is probably due to fast reaction rates either with cuticular surfaces or with mesophyll surfaces compared to molecular diffusion rates and should not be interpreted to suggest that red spruce would be tolerant to ozone at the levels examined in this work. A better understanding of the stomatal dimensions would clarify where the ozone disappears and give an indication as to which chemistry is more important (cuticular vs mesophyll). These calculations therefore suggest that, in order to obtain a reasonable estimate of the fate of reactive pollutants in the stomata, good estimates of the stomatal density and the stomatal dimensions should be obtained.

Losses to Non-Stomatal Surfaces. In H₂O₂ chamber experiments, losses to nonplant surfaces in the exposure chamber are high, even if relatively inert surfaces, such as Teflon, are used (13, 14). The fraction of the flux to needle surfaces which is attributed to decomposition on non-stomatal regions was estimated (14) to average $40 \pm 26\%$ for light-on conditions and $83 \pm 6\%$ for light-off conditions. The sensitivity of this model to the H₂O₂ flux was therefore also examined in this analysis. Reducing the H₂O₂ stomatal flux to 50% and to 10% of its base case value changed the location at which the H₂O₂ concentration goes to zero from 2 μm (base case) to 4 μm (i.e., still in the antechamber) (50%) to 17 μm (or nearing the top of the stomata) (10%). The sensitivity of this calculation to the H₂O₂ flux suggests that the decomposition of H₂O₂ on non-stomatal plant surfaces should be more closely examined.

Capillary Condensation. These simulations predicted that both SO₂ and H₂O₂ consistently disappeared in the porous wax plug (i.e., region III) without reaching the stomata. Furthermore, this result was found consistently during the sensitivity studies. This result is not unexpected for H₂O₂ since it is possible that H₂O₂ decomposes on the leaf surface and in the porous wax medium of region III. However, SO₂ has been observed to respond to stomatal activity (e.g., ref 49); therefore, SO₂ was expected to reach the stomata. Since the waxy material in the stomatal antechamber is typically assumed to be relatively inert, we examined the possibility that liquid water could equilibrate with water vapor in this region, thus providing a sink for SO₂ and H₂O₂. As the relative humidity of the surrounding air increases, adsorption of water vapor into porous media increases until the adsorbed water behaves like liquid water (refs 50 and 51, and references cited therein). The Kelvin equation was used to calculate the ratio of the equilibrium partial pressure of water vapor over a cylindrical meniscus of condensing water, P , to the

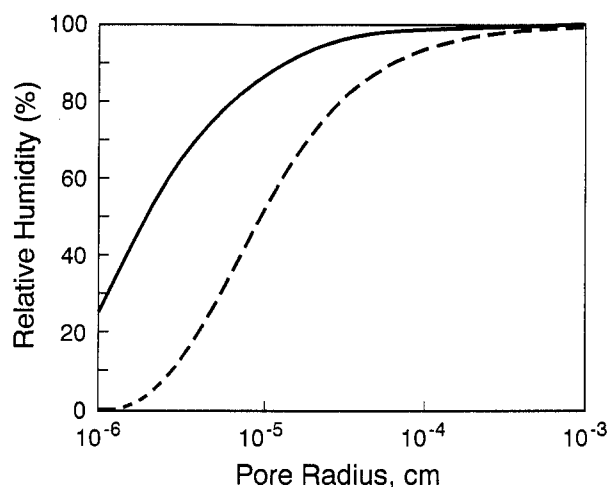


Figure 7. Critical relative humidity at which water condensation occurs, as a function of cylindrical meniscus radius, for stomatal antechamber. Calculated from the Kelvin equation. Solid line is for contact angle of 85°; dashed line is for 65°.

saturation vapor pressure over a flat surface, P_0 , given the meniscus radius r (cm) and the contact angle ϕ (51)

$$P/P_0 = \exp\left(-\frac{\sigma V \cos(\phi)}{rRT}\right) \quad (34)$$

where σ is the surface tension of water (at 20 °C, $\sigma = 72.88 \text{ erg cm}^{-2}$), V is the molar volume of liquid water ($18 \text{ cm}^3 \text{ mol}^{-1}$), T is in K, and R is the ideal gas constant ($8.314 \times 10^7 \text{ erg mol}^{-1} \text{ K}^{-1}$). Figure 7 shows the ratio P/P_0 as a function of the cylindrical meniscus radius for contact angles of 65° and 85°. Since the cutin is made up of the esters of carboxylic acids and contains 2–3 hydroxyl groups, this material is suspected of being slightly more hydrophilic than materials such as Teflon or polyethylene (52), for which contacts angle range from 94 to 117° (53).

For pore radii in the range of 0.1–1 μm (the range of dimensions in the antechamber) and contact angle in the range of 65–85°, the critical relative humidity is estimated to range from 60 to 90%. This range is similar to the relative humidity calculated in the base case at the bottom of the waxy plug region, which approaches 85% and 75% in the daytime and nighttime cases, respectively.

We interpret this to suggest that it may be possible for water to condense in the stomatal antechamber, thus providing a sink for water-soluble gases. For other vegetative species, fluxes of SO₂ have been observed to respond to stomatal aperture (i.e., lower fluxes observed during dark periods, e.g., ref 49). We recognize that liquid water would provide only a temporary sink for SO₂, because partitioning of SO₂ between the gas and liquid phases would eventually reach an equilibrium, unless an aqueous phase sink exists such as the presence of gaseous H₂O₂ which oxidizes SO₂ in the aqueous phase (e.g., ref 54). We speculate that in the experiments of Ennis *et al.* (13) the presence of H₂O₂ may have affected the fate of SO₂ in the needle. A similar phenomenon was observed by Van Hove *et al.* (49) during simultaneous exposure of bean plants to NH₃ and SO₂, during which the deposition to external surfaces was found to increase with increasing relative humidity and simultaneous exposure enhanced the deposition of both species. It would be interesting to examine the uptake by conifers of SO₂ alone and then in simultaneous exposures to determine whether the uptake of

SO₂ is affected by the presence of oxidative species with which it may react.

An examination of the relationship between the ambient relative humidity and the location at which H₂O₂ disappears for the data by Claiborn and Aneja (14) found no statistically significant correlation between these parameters, as might be expected from the above discussion; however, their experiments did not include a wide range of relative humidities. It appears that the H₂O₂ disappears relatively soon in the leaf, regardless of the relative humidity or the presence of other gases. The presence of light appears to enhance the loss process (Table VIII), since during the day the H₂O₂ disappeared sooner than during the night. We speculate that H₂O₂ decomposes on the surface of the spruce needle and that this decomposition is enhanced during the daytime conditions, either by the increased leaf temperature or by photolytic processes.

V. Summary and Conclusions

A mathematical model was developed to describe the transport of gases into conifer needles. The model was applied to the specific cases of O₃, SO₂, and H₂O₂ transport into needles of red spruce and takes into account the effects of photosynthesis, transpiration and respiration during daytime and nighttime conditions. The model considers multicomponent gas diffusion, heterogeneous chemical reactions inside the needle, and specific leaf geometry and stomatal features. The model was used to analyze two sets of experiments which studied the uptake of several reactive air pollutants by red spruce (13, 14). Although the model is not verifiable in its present formulation, its predictions of intercellular gaseous concentration profiles are reasonable and enlightening.

Unlike the typical deposition velocity model, which has been applied to leaves with a flat plate geometry, this model specifically takes into account the detailed anatomy of the leaf. Model calculations suggest that the wax plug of the stomatal antechamber offers a significant resistance to gas transport into and out of the stomatal region. During the day, this plug may provide a larger resistance to transport than the stomata. At night, although less important than the stomatal resistance as the pore closes, the wax plug nevertheless provides a significant resistance to gas exchange.

For the range of trace gas concentrations considered in this work ([SO₂] 8.6–10.4 ppb; [H₂O₂] = 3.3–3.9 ppb; [O₃] = 89–92 ppb), the model results indicate that during simultaneous exposure to trace gases O₃, H₂O₂, and SO₂, H₂O₂ and SO₂ seem to disappear before reaching the stomatal pore, suggesting that there is a sink for each of these species in the waxy antechamber. The results of our sensitivity analysis indicate that, depending on the accuracy of our estimates of stomatal dimensions, for the range of conditions considered in this work, it is possible that the O₃ may be reaching the substomatal zone where it would then disappear immediately due to chemical reactions in this region. During experiments in which spruce saplings were exposed only to H₂O₂, for chamber H₂O₂ concentrations ranging from 1.0 to 3.5 ppb, it appears that this gas also disappeared in the region above the stomata, consistent with the suggestion that H₂O₂ decomposes on external leaf surfaces. We speculate that, through capillary condensation, liquid water in the antechamber may provide the medium in which reactive,

water-soluble trace species may react. Further experimentation specifically investigating the sensitivity of the SO₂ flux to simultaneous exposure with other oxidants (such as O₃ and H₂O₂) followed by interpretation using this model could address this possibility.

For these studies (for [O₃] < 100 ppb) the internal concentration of O₃ approaches zero in the stomata, possibly close to the top of the substomatal zone. It is possible that either O₃ reacts so rapidly in the substomatal zone that the concentration is always zero or that there may be another sink in the waxy antechamber or in the stomata. If there is a sink for O₃ other than in the substomatal zone, it is apparently not as efficient as that for H₂O₂ or SO₂.

The results of our sensitivity studies indicate that, in order to accurately calculate the inner CO₂ concentration, very accurate measurements of the leaf temperature, chamber inlet and outlet air dewpoint temperature, and total chamber gas flow rate are required. In order to understand the fate of reactive and/or water-soluble trace gases, a good chemical characterization of the waxy plug as well as good estimates of all stomatal zone dimensions are needed. The assumption that the waxy cuticular material is inert does not appear to apply to gaseous H₂O₂ and may not apply to other gaseous species (such as SO₂ and O₃). The reactivity of the cuticular wax with these atmospheric trace gases, when exposed singularly or in the presence of other trace gases, should be further investigated.

Although these calculations suggested that, for all cases considered, the ozone concentration in the substomatal chamber appears to be zero, we point out that this should not be interpreted to suggest that the red spruce would be tolerant to ozone for the conditions examined in this work. In order to use this model to examine the implications of exposure to air pollutants for forest decline, more detailed information is needed on the chemistry and biochemistry of the specific air pollutant in plant tissues.

Acknowledgments

We gratefully acknowledge support made available to C.S.C. in the form of an assistantship from the Department of Chemical Engineering at North Carolina State University. The comments from anonymous reviewers were very helpful. We thank Dr. Robert Bruck, NCSU, for discussions on the needle physiology for red spruce and Dr. Michael Overcash, NCSU, for helpful discussions on this work. The late Dr. Ron Bradow, U.S. Environmental Protection Agency, was especially helpful in numerous discussions of this model. He will be sorely missed.

Literature Cited

- (1) Heck, W. W. In *Proceedings from the International Conference on Assessment of Crop Loss from Air Pollutants*, Raleigh, NC, Oct 25–29, 1987; Elsevier Applied Science: New York, 1987.
- (2) Woodman, J. N.; Cowling, E. B. *Environ. Sci. Technol.* 1987, 21, 120.
- (3) Lamb, B.; Guenther, A.; Gay, D.; Westberg, H. *Atmos. Environ.* 1987, 21, 1695.
- (4) Hill, A. C. *JAPCA* 1971, 21, 341.
- (5) Walcek, C. J. *Atmos. Environ.* 1987, 21, 2649.
- (6) Bennett, J. H.; Hill, A. C.; Gates, D. M. *JAPCA* 1973, 23, 957.
- (7) O'Dell, R. A.; Taheri, M.; Kabel, R. L. *JAPCA* 1977, 27, 1104.
- (8) Jarman, P. D. *J. Exp. Bot.* 1974, 25, 927.

- (9) Von Caemmerer, S.; Farquhar, G. D. *Planta* 1981, 153, 376.
- (10) Jackson, R. *Transport in Porous Catalysts*; Elsevier: Amsterdam, 1977.
- (11) Cunningham, R. E.; Williams, R. J. J. *Diffusion in Gases and Porous Media*; Plenum Press: New York, 1980.
- (12) Leuning, R. *Plant Cell Environ.* 1983, 6, 181.
- (13) Ennis, C. A.; Lazrus, A. L.; Zimmerman, P. R.; Monson, R. K. *Tellus* 1990, 42B, 183.
- (14) Claiborn, C. S.; Aneja, V. P. *Environ. Sci. Technol.* 1993, preceding paper in this issue.
- (15) Radford, A. E. *Manual of the Vascular Flora of the Carolinas*; University of North Carolina Press: Chapel Hill, NC, 1968.
- (16) Marco, H. F. *J. Agric. Res.* 1939, 58, 357.
- (17) Pielou, E. C. *The World of Evergreens*; Comstock Publishers and Associates: Ithaca, NY, 1988.
- (18) den Ouden, P.; Boom, B. K. *Manual of Cultivated Conifers Hardy in the Cold- and Warm-Temperature Zone*; Martinus Nijhoff: The Hague, 1978.
- (19) Jeffree, C. E.; Johnson, R. P. C.; Jarvis, P. G. *Planta* 1971, 98, 1.
- (20) Nobel, P. S. *Introduction to Biophysical Plant Physiology*; W. H. Freeman and Co.: San Francisco, 1974.
- (21) Bruck, R. I.; Robarge, W. P.; McDaniel, A. *Eur. J. For. Pathol.* 1989, 17, 528.
- (22) Hall, J. L. In *Plant Physiology: A Treatise, Vol. VII*; Steward, F. C., Ed.; Academic Press: New York, 1983; pp 3-156.
- (23) Newcomb, E. N. *Annu. Rev. Plant Physiol.* 1963, 14, 43.
- (24) Robinson, D. G.; Depta, H. *Annu. Rev. Plant Physiol.* 1988, 39, 53.
- (25) Castillo, F. J.; Miller, P. R.; Greppin, H. *Experientia* 1987, 43, 111.
- (26) Chameides, W. L. *Environ. Sci. Technol.* 1989, 23, 595.
- (27) Tingey, D. T.; Taylor, G. E., Jr. In *Effects of Gaseous Air Pollution in Agriculture and Horticulture*; Unsworth, M. H., Ormrod, D. D., Eds.; Butterworth Scientific: London, 1982; p 113.
- (28) Slattery, J. C. *Momentum, Energy, and Mass Transfer in Continua*; Robert E. Krieger Publishing Co.: New York, 1981.
- (29) Mason, E. A.; Evans, R. B., III. *J. Chem. Educ.* 1969, 46, 358.
- (30) Bird, R. B.; Stewart, W. E.; Lightfoot, E. N. *Transport Phenomena*; John Wiley and Sons: New York, 1960.
- (31) Zanolli, F.; Carbonell, R. G. *Chem. Eng. Sci.* 1983, 39, 299.
- (32) Perry, R. H.; Chilton, C. H., Eds. *Chemical Engineers' Handbook*; McGraw-Hill Book Co.: New York, 1973.
- (33) Present, R. D. *Kinetic Theory of Gases*; McGraw-Hill Book Co.: New York, 1958.
- (34) Farquhar, G. D.; Von Caemmerer, S.; Berry, J. A. *Plant* 1980, 149, 78.
- (35) Lind, J. A.; Kok, G. L. *J. Geophys. Res.* 1986, 91, 7889.
- (36) Jayne, J. T.; Gardner, J. A.; Davidovits, P.; Worsnop, D. R.; Zahniser, M. S.; Kolb, C. E. *J. Geophys. Res.* 1990, 95, 20559.
- (37) Carbonell, R. G.; Whitaker, S. *Chem. Eng. Sci.* 1983, 38, 1795.
- (38) Geankoplis, C. J. *Mass Transport Phenomena*; Holt, Rinehart and Winston: New York, 1972.
- (39) Kramer, P. J.; Kozlowski, T. T. *Physiology of Woody Plants*; Academic Press: New York, 1979.
- (40) Nobel, P. S. *Biophysical Plant Physiology and Ecology*; W. H. Freeman and Co.: San Francisco, 1983.
- (41) Beadle, C. L.; Jarvis, P. G.; Neilson, R. E. *Physiol. Plant.* 1979, 45, 158.
- (42) Grieu, P.; Guehl, J. M.; Aussenac, G. *Physiol. Plant.* 1988, 73, 97.
- (43) Laisk, A.; Kull, O.; Moldau, H. *Plant Physiol.* 1989, 90, 1163.
- (44) Mansfield, T. A.; Davis, W. J. *BioScience* 1985, 35, 158.
- (45) Sanford, A. P.; Jarvis, P. G. *Tree Physiol.* 1986, 2, 89.
- (46) Hanson, P. J.; McLaughlin, S. B. *J. Environ. Qual.* 1989, 18, 499.
- (47) Pier, P. A.; Thornton, F. C.; McDuffie, C., Jr.; Hanson, P. J. *Environ. Exp. Bot.* 1992, 32, 115.
- (48) McLaughlin, S. B.; Andersen, C. P.; Hanson, P. J.; Tjoelker, J. G.; Roy, W. K. *Can. J. For. Res.* 1991, 21, 1234.
- (49) Van Hove, L. W. A.; Van Kooten, O.; Adema, E. H.; Vredenberg, W. J.; Pieters, G. A. *Atmos. Environ.* 1989, 23, 2515.
- (50) Fisher, L. R. *Adv. Colloid Interface Sci.* 1982, 16, 117.
- (51) Camuffo, D. *Water, Air, Soil Pollut.* 1984, 21, 151.
- (52) Schonherr, J. *Planta* 1976, 128, 113.
- (53) Pruppacher, H. R.; Klett, J. D. *Microphysics of Clouds and Precipitation*; D. Reidel Publishing Co.: Dordrecht, Holland, 1980.
- (54) Penkett, S. A.; Jones, B. M. R.; Brice, K. A.; Eggleton, A. E. *J. Atmos. Environ.* 1979, 13, 123.

Received for review May 25, 1993. Accepted June 23, 1993.*

* Abstract published in *Advance ACS Abstracts*, August 15, 1993.